ACS Catalysis

Review

pubs.acs.org/acscatalysis

Review on Recent Progress in Nitrogen-Doped Graphene: Synthesis, Characterization, and Its Potential Applications

Haibo Wang, Thandavarayan Maiyalagan, and Xin Wang*

School of Chemical and Biomedical Engineering, Nanyang Technological University, 62 Nanyang Drive, Singapore, 637459

ABSTRACT: Nitrogen doping has been an effective way to tailor the properties of graphene and render its potential use for various applications. Three common bonding configurations are normally obtained when doping nitrogen into the graphene: pyridinic N, pyrrolic N, and graphitic N. This paper reviews nitrogen-doped graphene, including various synthesis methods to introduce N doping and various characterization techniques for the examination of various N bonding configurations. Potential applications of N-graphene are also reviewed on the basis of experimental and theoretical studies.

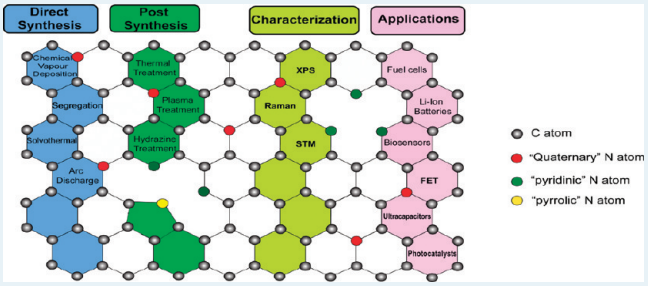

KEYWORDS: *graphene, nitrogen doping, electrocatalysis, field-effect transistor, energy storage*

1. INTRODUCTION

Graphene is a novel nanomaterial with a single sheet of carbon atoms packed in a hexagonal lattice. Since the first report of its synthesis via a "Scotch tape" method in 2004,[1] graphene has emerged as one of the most active research fields. The fascinating properties of graphene, such as high surface area (2630 m^2/g),[2] high thermal conductivity (~5000 W/mK),[3] fast charged carrier mobility (~200 000 cm^2 V^{-1} s^{-1})[3] and strong Young's modulus (~1 TPa),[4] have been well documented. Various morphologies have also been obtained, including two-dimensional graphene nanosheets (GNSs), one-dimensional graphene nanoribbons (GNRs),[5−7] and zero-dimensional graphene quantum dots (GQDs).[8,9] The properties of GNRs and GQDs can be tuned by their size and edges. For instance, GNRs with width narrower than 10 nm showed obvious semiconducting characteristics, but GNRs with width larger than 10 nm exhibited very weak gate dependence.[10] The increased concentration of a zigzag edge tended to decrease its band gap.[9] All these aspects make graphene material promising for various applications, including energy conversion and storage, electrocatalysis, sensors and electronics.

Other than morphology control, chemical doping is another important approach to tailor the property of graphene, which has been proved effective in the doping of carbon nanotubes (CNTs) and greatly broadened their applications.[11−15] Usually, there are two means to chemically dope graphene: (1) the adsorption of gas,[16] metal,[17] or organic molecules[18] to the graphene surface and (2) substitutional doping, which introduces heteroatoms, such as nitrogen atoms and boron atoms, into the carbon lattice of graphene. Both of these methods can modulate the electronic properties of graphene. In this paper, our focus will be constrained to the topic of nitrogen-doped graphene (N-graphene).

When a nitrogen atom is doped into graphene, it usually has three common bonding configurations within the carbon lattice, including quaternary N (or graphitic N), pyridinic N, and pyrrolic N (Figure 1). Specifically, pyridinic N bonds with

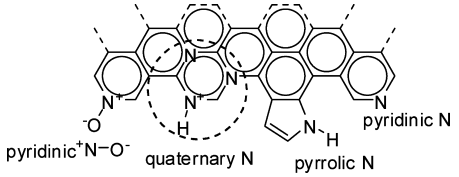

Figure 1. Bonding configurations for nitrogen atoms in N-graphene.[24]

two C atoms at the edges or defects of graphene and contributes one p electron to the π system. Pyrrolic N refers to N atoms that contribute two p electrons to the π system, although unnecessarily bond into the five-membered ring, as in pyrrole.[19,20] Quaternary N refers to N atoms that substitute for C atoms in the hexagonal ring. Among these nitrogen types, pyridinic N and quaternary N are sp^2 hybridized and pyrrolic N is sp^3 hybridized. Apart from these three common nitrogen types, N oxides of pyridinic N have been observed in both the N-graphene and N-CNT studies.[21−23] In this configuration, the nitrogen atom bonds with two carbon atoms and one oxygen atom.

The N-graphene shows different properties compared with the pristine graphene. For instance, the spin density and charge distribution of carbon atoms will be influenced by the neighbor nitrogen dopants,[25,26] which induces the "activation region" on the graphene surface. This kind of activated region can participate in catalytic reactions directly, such as the oxygen

Special Issue: Electrocatalysis

Received: December 12, 2011
Revised: February 23, 2012
Published: March 16, 2012

   dx.doi.org/10.1021/cs200652y | *ACS Catal.* 2012, 2, 781−794

Table 1. Nitrogen-Doping Methods and Nitrogen Concentration on Graphene

no.	synthesis method	precursors	N content, at. %	application/ reference
1	CVD	Cu film on Si substrate as catalyst, CH_4/NH_3	1.2−8.9	FET[30]
2	CVD	Cu foil as catalyst, NH_3/He	1.6−16	ORR[40]
3	CVD	Ni film on SiO_2/Si substrate as catalyst, $NH_3/CH_4/H_2$/Ar (10:50:65:200)	4	ORR[41]
4	CVD	Cu foil as catalyst, acetonitrile	∼9	lithium battery[43]
5	CVD	Cu foil as catalyst, pyridine	∼2.4	FET[44]
6	segregation growth	carbon-contained Ni layer on nitrogen-contained boron layer	0.3−2.9	FET[50]
7	solvothermal	Li_3N/CCl_4 (NG1) or $N_3C_3Cl_3/Li_3N/CCl_4$ (NG2)	4.5 (NG1) or 16.4 (NG2)	ORR[52]
8	arc discharge	graphite/H_2/He/pyridine (NG1) graphite/H_2/He/NH_3 (NG2) transformation of nanodiamond/He/pyridine (NG3)	0.6 (NG1), 1 (NG2), 1.4 (NG3)	56, 57
9	thermal treatment	N^+ ion-irradiated graphene, NH_3	1.1	FET[59]
10	thermal treatment	graphite oxide after thermal expansion, NH_3/Ar	2.0−2.8	ORR[60]
11	thermal treatment	GNR, NH_3		FET[31]
12	thermal treatment	GO, NH_3/Ar (10% NH_3)	∼3−5	FET[63]
13	thermal treatment	GO, NH_3	6.7−10.78	methanol oxidation[73]
14	thermal treatment	GO, melamine	7.1−10.1	ORR[62]
15	plasma treatment	graphite oxide after thermal expansion, N_2 plasma	8.5	ORR[23]
16	plasma treatment	graphite oxide after thermal expansion, N_2 plasma	3	ORR[67]
17	plasma treatment	chemically synthesized graphene, N_2 plasma	∼1.3	biosensors[68]
18	plasma treatment	GO, treat with H_2 plasma first, then treat with N_2 plasma	1.68−2.51	ultracapacitor[69]
19	plasma treatment	mechanically exfoliated graphene or bilayer graphene grown by CVD, NH_3 plasma		FET[70]
20	N_2H_4 treatment	GO, N_2H_4, NH_3	4.01−5.21	71
21	N_2H_4 treatment	graphite oxide after thermal expansion, N_2H_4	1.04	electrochemical sensor[72]

reduction reaction (ORR), or anchor the metal nanoparticles used in the catalytic reaction. Moreover, after nitrogen doping in the monolayer graphene, the Fermi level shifts above the Dirac point,[27,28] and the density of state near the Fermi level is suppressed;[29,30] thus, the band gap between the conduction band and the valence band will be opened. For GNRs, the band gap is still kept after doping.[31] The band gap in N-graphene makes it a candidate to be used in semiconductor devices. Apart from these, N-graphene can also be used in batteries, sensors, and ultracapacitors. The nitrogen doping of graphene greatly broadens its applications.

Previously, several reviews on graphene have mentioned N-graphene,[32−35] especially the review of Liu et al.,[35] which focused on two chemical doping approaches and band gap tuning; however, there is still no systematical study of N-graphene synthesized by substitutional doping. Therefore, in this review, we summarize different synthesis and characterization methods of nitrogen-substituted graphene; the application of N-graphene is also reviewed on the basis of experimental and theoretical studies.

2. SYNTHESIS OF N-GRAPHENE

Similar to the synthesis of N-CNT, N-graphene can be obtained through two different ways: direct synthesis and post treatment. Most postsynthesis treatments may lead to surface doping only. Although in principle, direct synthesis may have the potential to create a homogeneous doping throughout the bulk material, the results reported so far fail to indicate so. Specifically, direct synthesis includes chemical vapor deposition (CVD), segregation growth, solvothermal, and arc-discharge approaches. Post treatment includes thermal treatment, plasma treatment, and N_2H_4 treatment. Table 1 gives a summary of various methods used for the synthesis of N-graphene. Detailed discussion on these methods is elaborated below.

2.1. Direct Synthesis. *2.1.1. CVD Approach.* CVD is a widely used method to synthesize various carbon nanomaterials, such as graphene,[36] CNTs,[37] carbon nanofibers,[38] and N-doped CNTs.[39] Recently, it was successfully applied to prepare N-graphene. Typically,[30,40,41] a metal catalyst (Cu or Ni) is used as the substrate, then at high temperature, a carbon source gas mixed with a nitrogen-containing gas is introduced. These precursors dissociate and recombine into N-graphene by means of precipitation on the surface of the catalyst.[30,42]

Apart from the gas mixture, liquid organic precursors (acetonitrile, pyridine) have also been used to form N-graphene.[43,44] Theoretical study about different precursors[45] shows that proper skeletal bonds of liquid precursors are crucial for the formation of N-graphene. Acrylonitrile containing the C−C single bond, C═C double bond, and C≡N triple bond cannot form N-graphene, but pyridine with only the double bond forms N-graphene. The proposed reason is that the single bond is easy to break, even at low temperature, leaving C═C and C≡N bonds at the catalyst surface. Then C≡N bond is

dx.doi.org/10.1021/cs200652y | ACS Catal. 2012, 2, 781−794

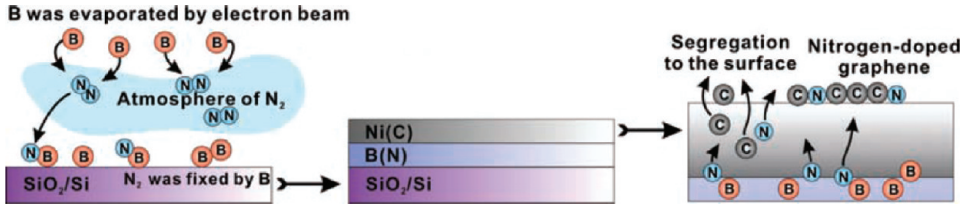

Figure 2. Schematic illustration of the segregation technique for growing N-doped graphene.[50]

preferentially removed from the surface by forming volatile molecules when the temperature is higher than 400 °C; thus, only C═C will be left to form nondoped graphene above 500 °C. In contrast, the skeletal bonds in pyridine have similar bond energies, which induces the formation of N-graphene.

The layer distribution of N-graphene is varied in different studies. Although the N-graphene synthesized from the gas mixture C_2H_4/NH_3 is claimed to be monolayer through the analysis of Raman spectroscopy,[40] N-graphene synthesized from a gas mixture, CH_4/NH_3,[30,41] shows that the few-layer graphene is predominant after high-resolution transmission electron microscope (HRTEM) characterization. In other studies, monolayer N-graphene is also obtained when acetonitrile[43] or pyridine[44] is used as precursors. Furthermore, the layer of N-graphene can be adjusted by the flowing time if acetonitrile is used as the precursor.[43]

In the CVD approach, the nitrogen content can be controlled by changing the flow rate[40] and the ratio between carbon source and nitrogen source.[30] It has been reported[30] that the doping level decreased from 8.9 to 3.2 or 1.2 at. % if the NH_3/CH_4 ratio was lowered from 1:1 to 1:2 or 1:4, respectively. Moreover, although high nitrogen content (~16 at. %) has been reported,[40] the nitrogen content in this method is normally around 4−9 at. %.

The bonding configuration of nitrogen within N-graphene varies with different studies. By using Cu as the catalyst and CH_4/NH_3 (1:1) as the precursor, the nitrogen type in N-graphene is mainly quaternary N;[30] however, when Ni is used as the catalyst and CH_4/NH_3 (5:1) is used as the precursor, the obtained N-graphene consists of mainly pyridinic N and pyrrolic N.[41] If C_2H_4/NH_3 is used as the precursor while keeping Cu as the catalyst, the pyridinic N becomes the predominant type.[40] Notably, the syntheses of other nitrogen-doped carbon materials have revealed that the doping environment is also influenced by the flow rate, catalyst, and growth temperature,[46−49] so further research is required to clarify the relationship between the bonding configuration of nitrogen and the parameters of CVD.

2.1.2. Segregation Growth Approach. In this approach, a nitrogen-containing boron layers and carbon-containing nickel layers are sequentially deposited on the SiO_2/Si substrate by electron beam evaporation, then during the vacuum annealing process, the boron atoms are trapped by nickel, and the carbon atoms will segregate out onto the nickel surface and combine to form N-graphene (Figure 2).[50] Although sporadic multilayer areas are observed, the N-graphene generally shows a large-scale, uniform, and few-layer structure. The nitrogen content (0.3−2.9 at. %) can be controlled by adjusting the thickness of the boron and nickel films. The pyridinic and pyrrolic N are dominant in N-graphene. Interestingly, the graphene can be doped in a specific area by embedding nitrogen species into the selective area of the substrate.

2.1.3. Solvothermal Approach. The solvothermal approach was first employed for gram-scale production of graphene.[51] Recently, gram-scale production of N-graphene has been achieved by applying this approach at ~300 °C. By mixing lithium nitride (Li_3N) with tetrachloromethane (CCl_4) (Figure 3) or cyanuric chloride ($N_3C_3Cl_3$) with Li_3N and CCl_4, N-

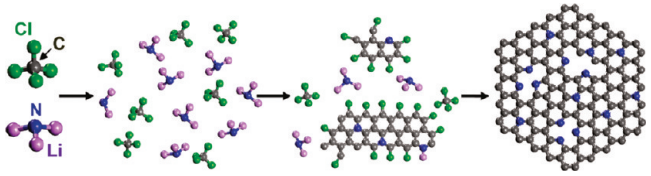

Figure 3. Schematic illustration for N-graphene synthesized from the reaction of CCl_4 and Li_3N.[52]

graphene with different nitrogen contents was obtained (denoted as NG1 and NG2, respectively).[52] The HRTEM images of N-graphene show that it mainly consists of 1−6 layer graphene. Because of the introduction of $N_3C_3Cl_3$, NG2 has a higher nitrogen content (16.4 at. %) compared with NG1(4.5 at. %). The proportion of doped nitrogen species also changes with different reactant mixtures. The quaternary N dominates in NG1, and pyridinic and pyrrolic N dominates in NG2.

2.1.4. Arc-Discharge Approach. An arc-discharge approach has been applied to obtain CNTs and doped CNTs by evaporating the carbon source, normally graphite,[53−55] at high temperature. Rao et al.[56,57] successfully obtained N-graphene by applying this method in the presence of pyridine vapor or NH_3. The N-graphene synthesized from transformation of nanodiamond shows higher nitrogen content than that synthesized from graphite. The nitrogen content of the as-synthesized N-graphene is around 0.5−1.5 at. %. Moreover, although single layer N-graphene is occasionally observed, most of the N-graphene possesses two or three layers. The scale of graphene and N-graphene produced by this method normally is below 1 μm.[56,58]

2.2. Postsynthesis Treatment. *2.2.1. Thermal Treatment.* Thermal treatment refers to the method using high temperature to produce N-graphene. It has been shown that heating graphene in NH_3 at high temperature (≥800 °C) can produce N-graphene.[59,60] Electrical annealing, which produces high temperature, has also been applied to obtain N-GNRs.[31] The nitrogen content in the N-graphene synthesized by this method is relatively low. Guo et al.[59] obtained N-graphene with 1.1 at. % doping level at 1100 °C; Geng et al.[60] reported that the highest nitrogen content was 2.8 at. % at 800 and 900 °C. The low doping level may be attributed to two reasons: one is the insufficient defect number in the high quality graphene, and the other is the high annealing temperature, which will break the C−N bonds in N-graphene.[61] Moreover, the nitrogen doping is more likely to occur at the defects and edge of graphene in the thermal treatment method. Geng et al.[60] found

dx.doi.org/10.1021/cs200652y | ACS Catal. 2012, 2, 781−794

pyridinic and pyrrolic N dominated in the N-graphene. Wang et al.[31] claimed that nitrogen atoms preferred functionalizing the edge of GNRs. Interestingly, unlike NH_3, annealing N^+ ion irradiated graphene in N_2 at high temperature cannot introduce nitrogen into the graphene,[59] which suggests that the inertness of N_2 makes it difficult to react with the reactive carbon atoms on the defect sites in graphene.

Apart from graphene, graphene oxide can also be used to synthesize N-graphene by thermal treatment in the presence of various nitrogen precursors. Sheng et al.[62] reported that annealing GO in the presence of melamine at high temperature (700−1000 °C) could produce N-graphene. The layer distribution of N-graphene depends on the synthesis procedure. Few-layer N-graphene is obtained if annealing the mixture of GO and melamine at high temperature, and single layer N-graphene can be produced if heating single-layer GO covered with melamine. The nitrogen content is affected by both the temperature and the mass ratio between GO and melamine. The largest nitrogen content (10.1 at. %) is obtained under 700 °C when the mass ratio of GO to melamine is 0.2. Li et al.[63] showed that placing GO in an NH_3 atmosphere through thermal annealing (500 °C) could reduce GO and get N-graphene with a 5 at. % nitrogen doping level. Notably, both of these works report that the temperature has the major influence on the nitrogen content of N-graphene. Li et al.[63] ascribed the reason to the decreased content of oxygen functional groups at higher temperature. Because these oxygen functional groups are responsible for the formation of a C−N bond, the reactivity between GO and nitrogen atoms will decrease after these groups decompose at higher temperature, resulting in the lower nitrogen content. Moreover, it has been claimed that lowering the mass ratio between GO and melamine at 800 °C induced higher nitrogen doping level, which may suggest the competitive doping between oxygen and melamine.[62]

2.2.2. Plasma Treatment. When carbon material is placed in the nitrogen plasma atmosphere, carbon atoms will be partly replaced by nitrogen atoms; therefore, this method was applied to synthesize N-CNTs.[64−66] Recently, it has been reported that N-graphene could be prepared from graphene[23,67,68] or GO[69] by exposing it to the nitrogen plasma. NH_3 plasma has also been used to obtain N-graphene from mechanically exfoliated graphene .[70] The nitrogen content, which can be controlled by the plasma strength and exposure time, varies from 3 to 8.5 at. % in different works. During the plasma exposure process, defects and oxygen-containing groups are created.[23,68] Shao et al.[23] showed that graphene contains 3.5 at. % oxygen species while the N-graphene contains 8.6 at. % oxygen species, Wang et al.[68] reported that the content of oxygen species increased from about 15 to 26−28 at. % after doping. These results indicate the plasma treatment introduces a significant amount of oxygen species into graphene. The reason may be ascribed to the reactive carbon atoms at the edge of defects that are created by the plasma treatment.[23] Notably, in the N_2 plasma treatment, overexposure may decrease the electrocatalytic activity of N-graphene.[68] It has been reported that if graphene was exposed to the N_2 plasma over 40 min, the reduction current of H_2O_2 would decrease because of the destruction and split of the graphene plane.

2.2.3. Hydrazine Hydrate (N_2H_4) Treatment. Using hydrazine hydrate to prepare graphene from GO is a widely used method. Recently, N-graphene has been obtained by reducing GO in the NH_3 and N_2H_4 mixed solution.[71] The nitrogen content reaches up to 5 at. % when the reduction temperature is 80 °C; however, the absorbed N_2H_4 takes a non-negligible proportion in the total nitrogen content. If the reaction temperature rises to 160 °C or higher, the N_2H_4 will be desorbed and the nitrogen content decreases to ∼4 at. %. Interestingly, the morphology of N-graphene also changes with the temperature. The relative flat N-graphene is generated if GO is reduced at low temperature (≤120 °C), whereas the obvious agglomeration in N-graphene will occur if the temperature is higher.

By using ultrasonication,[72] N-graphene can be synthesized from graphene in the presence of N_2H_4. The agglomerated regions are also observed after doping. The nitrogen content is around 1 at. %. In addition to these, the nitrogen species in the N-graphene contains only pyridinic and pyrrolic nitrogen. The content and bonding configuration of nitrogen indicates the nitrogen atoms can be introduced only to the graphene edges and defects in this method.

3. CHARACTERIZATION TECHNIQUES FOR STUDYING NITROGEN-DOPED GRAPHENE

3.1. X-ray Photoelectron Spectroscopy (XPS) Technique. XPS is the standard technique to study the nitrogen-doping effect in graphene. In the XPS spectrum of N-graphene, the peaks appearing at about 400 and 284 eV correspond to the N1s and C1s, respectively. The ratio of peak intensity between N1s and C1s is used to determine the nitrogen content in N-graphene. Moreover, the N1s spectrum is used to determine the nitrogen configurations. In the research about N-graphene, the N1s spectrum usually can be deconvoluted to several individual peaks that are assigned to pyridinic N (398.1−399.3 eV), pyrrolic N (399.8−401.2 eV), and quaternary N (401.1−402.7 eV) (Figure 4). The peak position of these nitrogen types

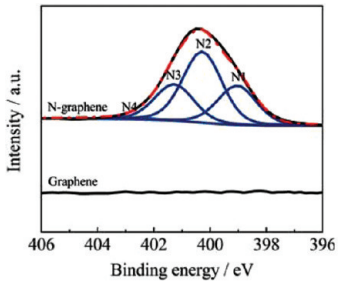

Figure 4. High-resolution N1s XPS spectra of graphene and N-graphene. N1 represents pyridinic N, N2 represents pyrrolic N, N3 represents quaternary N, and N4 represents the N oxides of pyridinic N.[23]

varies in a relatively wide range in different studies. Reddy et al.[43] reported the pyrrolic N appeared at 401.2 eV, whereas Li et al.[63] showed the quaternary N appeared at about 401.1 eV. The large difference of the peak positions of nitrogen configurations may be due to the different environments of nitrogen.[19] The charge of nitrogen and its neighbor atoms and the electron redistribution after ionization will all influence the precise position of different nitrogen types. Apart from these three nitrogen types, peak corresponding to N-oxides of pyridinic N is observed at ∼402.8 eV in several studies.[23,62]

When nitrogen atoms are doped into graphene, peaks at the C1s spectrum will change accordingly.[50,62,63,70,71] In the C1s spectrum of GO (Figure 5a), the sharp peak at around 284.5 eV corresponds to the sp^2 carbon with C═C bonds. Another strong peak at higher energy corresponds to the sp^3 carbon

dx.doi.org/10.1021/cs200652y | ACS Catal. 2012, 2, 781−794

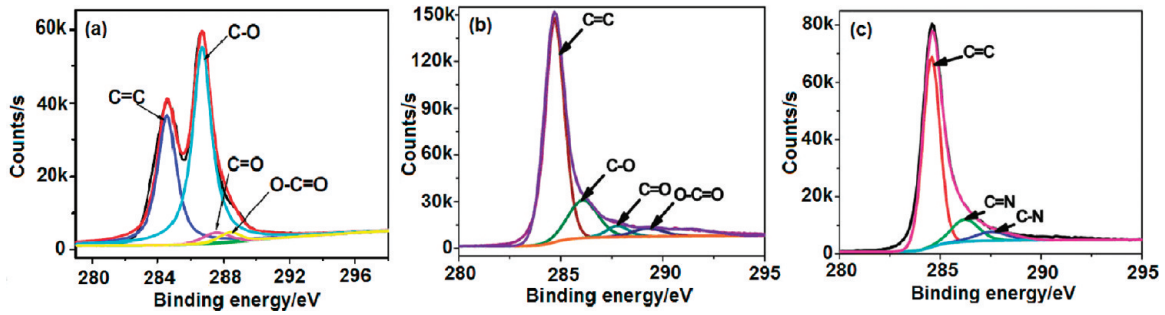

Figure 5. High-resolution C1 spectra of the (a) GO, (b) graphene prepared by annealing GO in Ar at 800 °C, and (c) N-graphene prepared by annealing GO/melamine (1:5) at 800 °C for 30 min.[62]

with several different C−O bonding configurations. These configurations include the C−O bonds, carbonyls (C═O), and carboxylates (O═C−O) at about 286.2, 287.8, and 289.2 eV, respectively. After GO is annealed in Ar, the intensity of the peak ascribed to the C−O bonding configurations decreases to a much lower value (Figure 5b).[62] This indicates that most of the oxygen groups in GO are removed after annealing. If GO is doped with nitrogen atoms (Figure 5c), peaks ascribed to C−O bonding configurations disappear, and new small peaks appear after peak fitting.[50,62,70,71] In the work of Sheng et al.,[62] new peaks appearing at 285.8 and 287.5 eV were assigned to the sp^2 and sp^3 carbon atoms, respectively. In other works,[50,70] a new small peak at ~289 eV was observed. This peak is ascribed to the physisorbed oxygen on the graphene. Generally speaking, the peak change at higher energy in the C1s spectrum suggests the nitrogen doping occurs in the graphene.

3.2. Raman Spectroscopy. Raman spectroscopy is another very useful method to characterize N-graphene. The D, G, and 2D bands are the predominant features in the spectrum of N-graphene. They are represented by peaks at around 1320−1350, 1570−1585, and 2640−2680 cm^{-1}, respectively (Figure 6.) In some studies,[40,52] the peak called D′ will appear at

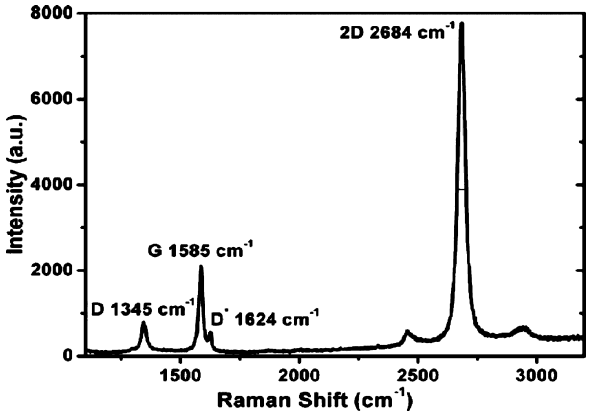

Figure 6. Typical Raman spectrum of N-graphene transferred onto a SiO_2/Si substrate. The laser excitation wavelength is 514.5 nm.[44]

~1602−1625 cm^{-1}. These bands already have been studied intensively in former studies.[74−78] Specifically, the G band corresponds to the doubly degenerate E_{2g} phonons at the Brillouin zone. It originates from the first-order Raman scattering process. The 2D and D bands are all induced by the second-order, double-resonance process and related to zone-boundary phonons. The scattering process involves two zone-boundary phonons for 2D mode; it involves one phonon and one defect for the D mode. Different from the D band which requires defects to activate it, the 2D band does not require the activation of defects. Thus, the 2D band is always seen in the Raman spectra of graphene and N-graphene, even when the D band cannot be observed. For the D′ band, it arises from the intravalley, defect-induced, double-resonance process.

Previous studies[77,79] have revealed that the intensity ratio of the D and G bands (I_D/I_G) was inversely proportional to the in-plane crystallite sizes L_a. The crystallite size can be determined according to the Tuinstra−Koenig (TK) relation, $L_a(nm) = (2.4 \times 10^{-10})\ \lambda^4 (I_D/I_G)^{-1}$ (λ is the Raman excitation wavelength). For nitrogen doping, the substitution of nitrogen atoms usually is accompanied by the introduction of defects into the graphene surface. Considering L_a as the average interdefect distance, more defects undoubtedly means a smaller L_a; thus, L_a can be used to study defects introduced by nitrogen doping. Comparing the crystallite size of pristine graphene with N-graphene, Zhang et al.[50] reported that the I_D/I_G of graphene and N-graphene with lower (NG1) and higher (NG2) nitrogen doping level are 0.26, 0.8 and 2.1, which corresponds to crystallite sizes of 65, 21, and 8 nm, respectively (Figure 7).

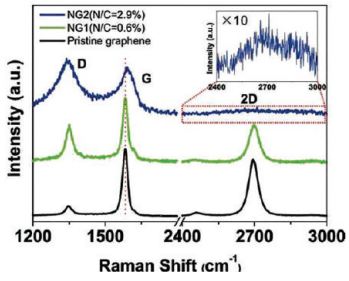

Figure 7. Raman spectra of pristine graphene and N-graphene with 0.6 (NG1) and 2.9 (NG2) at. % doping level. The insert shows the enlarged 2D band of NG2. The laser excitation wavelength is 514.5 nm.[50]

This suggests the crystallite size decreases remarkably with an increase in the nitrogen doping level because of the defects.

Apart from I_D/I_G, the intensity ratio of the 2D and G bands (I_{2D}/I_G) has been used to characterize N-graphene. It has been reported that I_{2D}/I_G depends on the electron concentration (Figure 8).[80] The G band always stiffens, and the 2D band responds differently to hole and electron doping; thus, I_{2D}/I_G has been used to estimate the nitrogen doping level.[50,70] Through calculating the I_{2D}/I_G, which was <0.6 in N-graphene, it was concluded that the doping level was higher than 4×10^{13} cm^{-2}.[50] Notably, some studies also presented that the G band increased almost linearly, corresponding to the increment of

dx.doi.org/10.1021/cs200652y | ACS Catal. 2012, 2, 781−794

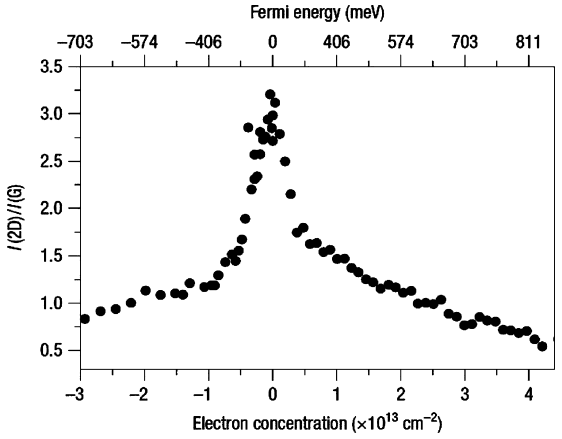

Figure 8. The influence of hole and electron doping on the I_{2D}/I_G.[80]

graphene layers,[81] and I_G/I_{2D} was related to the thickness of the graphene.[82,83] Thus, for N-graphene with inhomogeneous layers, the I_{2D}/I_G cannot reflect the nitrogen doping level. I_{2D}/I_G can be used only when N-graphene has homogeneous layers.

Before using I_D/I_G and I_{2D}/I_G to characterize N-graphene, inhomogeneous nitrogen doping should be considered. It has been reported that some spots showed high I_D/I_G and some showed very low I_D/I_G within the N-graphene,[40] which suggests the nonuniform defect distribution induced by inhomogeneous nitrogen incorporation. Thus, the I_D/I_G and I_{2D}/I_G derived from the Raman spectra at discrete spots cannot fully reflect the doping situation. In practice, Raman spectral mapping can be used to avoid this problem. This technique records the Raman spectra on a large scale; thus, the comparison of different N-graphenes is more convincing for inhomogeneous doping. In the maps of I_{2D}/I_G over a 80 × 80 μm^2 area (Figure 9b),[84] the pristine graphene shows a higher I_{2D}/I_G, which means a lower carrier concentration. The more area of low I_{2D}/I_G in N-graphene grown under higher NH_3 ratio corresponds to a higher carrier concentration. Moreover, it is observed that the size of the purple paths depends on the doping level, which indicates the purple paths are related to the local dopant concentration.

Some studies reported a shift of the G band after nitrogen doping. Because the variation of charge density in pristine graphene will cause the different G band positions and I_{2D}/I_G in the different spots of graphene,[85] Li et al. made a gold marker in the vicinity of graphene to accurately monitor the evolution of the nitrogen doping.[70] An upshift of the G band in the Raman spectra of the monolayer graphene was observed. In the work of Zhao et al.,[84] a similar trend of the G band was also observed by using the frequency histogram collected from Raman spectral mapping (Figure 9d). However, the observed position of the G band can also be affected by the inhomogeneous layer distribution[82,86] and defects due to nitrogen doping,[87] which may induce the downshift of G band in N-graphene in some studies.[52,63] Thus, comprehensive consideration should be taken if discussing this phenomenon.

3.3. Scanning Tunneling Microscopy (STM). STM is a very powerful technique to investigate the electronic properties of a sample. It can probe the charge density at the Fermi level. When the bias voltage (V_{bias}) applied between the tip and sample is positive, electrons tunnel from the tip into the specimen, then the lowest unoccupied states of the specimen are probed. When a negative V_{bias} is applied, electrons tunnel from the specimen into the tip, and the highest occupied states of specimen are probed.[88] Due to the sharp tip, the STM images can show atomic resolution. Recently, both theoretical and experimental studies on the electronic properties of N-graphene have been carried out.[52,84,89]

Compared with the pristine graphene, N-graphene shows some brighter sections that are distinct from the main graphene network in the STM image (Figure 10c).[52,84] Different bright features correspond to different nitrogen doping types. Because these bright sections are only a few atoms across (<1 nm), they cannot be defects induced by nitrogen doping.[52] Through the STM line scan over the bright section and graphene lattice (Figure 10a), an out-of-plane height of 0.6 ± 0.2 Å is observed. This indicates the substitution of nitrogen atoms in graphene. The calculated STM image shows that the C atoms neighboring

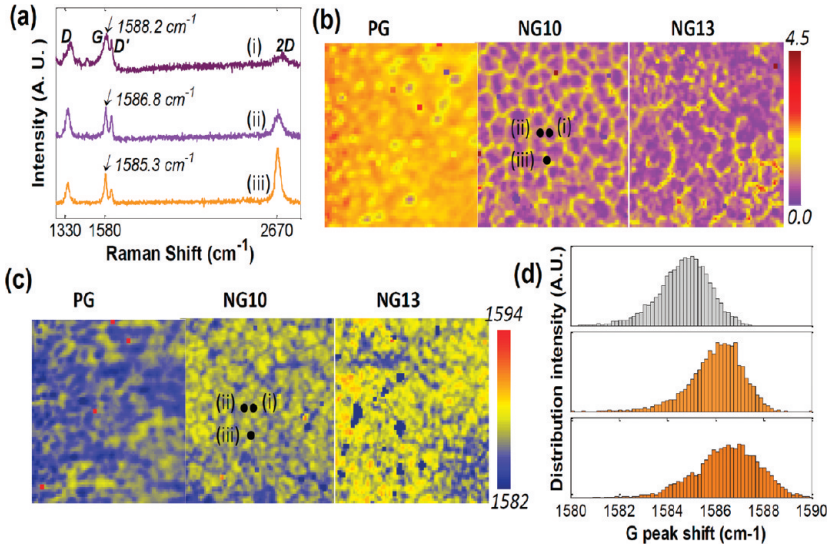

Figure 9. (a) Raman spectra taken at different positions over N-graphene grown under 0.1 Torr NH_3 (NG10). (b) Maps of I_{2D}/I_G for pristine graphene, NG10, and N-graphene grown under 0.13 Torr NH_3 (NG13). (c) Maps of the G band frequency for PG, NG10, and NG13 samples. (d) G band frequency histogram of PG, NG10, and NG13 from the maps in part c.[84]

dx.doi.org/10.1021/cs200652y | ACS Catal. 2012, 2, 781−794

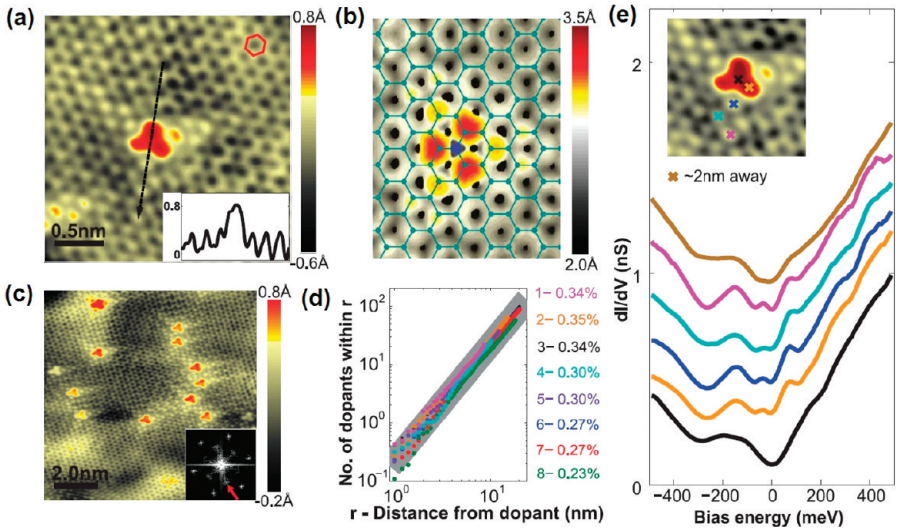

Figure 10. (a) STM image of the most common doping form in N-graphene. The inset is the line profile across the dopant (V_{bias} = 0.8 V, I_{set} = 0.8 nA). (b) Simulated STM image of quaternary N dopant based on density functional theory calculations (V_{bias} = 0.5 V). (c) STM image of N-graphene showing ~14 quaternary N dopants. The inset is the FFT of topography (V_{bias} = 0.8 V, I_{set} = 0.8 nA). (d) Spatial distribution of N−N distances from eight samples with different nitrogen concentrations. (e) dI/dV curves taken from an N atom and other nearby bright topographic features (V_{bias} = 0.8 V, I_{set} = 1.0 nA).[84]

N atoms exhibit the brightest feature because of the increased charge density of state induced by the neighbor N atoms (Figure 10b).[52,84]

Apart from the local structure around dopants, some long "tails" arising from the intervalley electron scattering are observed in the STM image (Figure 10c). This kind of scattering is verified by the inner hexagon in the fast Fourier transform (FFT). STM is also used to study the possibility of dopant clustering. The dopant distribution in the N−N distance is quadratic even when the distance is down to few lattice constants (Figure 10d); it indicates that the dopants distribute randomly. Furthermore, the study reveals that nearby dopants prefer to substitute into the same sublattice of graphene. The charge-carrier density of N-graphene can be measured from a STM study. From the curves of dI/dV (derivative of current with respect to the voltage), the Dirac point of N-graphene is calculated (Figure 10e). Then the charge-carrier density can be calculated from the relation $\mathbf{n} = E_D^2/\pi(\hbar v_F)^2$ ($\mathbf{n}$ is the charge-carrier density, $\hbar$ is the Plank's constant over 2π, ν_F is the Fermi velocity).

3.4. Other Characterization Techniques. In addition to the above techniques, scanning electron microscope (SEM), HRTEM, atomic force microscope (AFM), selected area electron diffraction (SAED) and thermogravimetric analysis (TGA) have also been used to study N-graphene. Specifically, SEM is commonly employed to study the morphology of N-graphene. HRTEM is the most commonly used technique to determine the number of graphene layers on the basis of the cross section or edge images of N-graphene. AFM can also be used to estimate the number of graphene layers on the basis of the interlayer distance. SAED can provide information about the crystalline structure of N-graphene on the basis of diffraction pattern. The hexagonal diffraction spots indicate that the N-graphene still keeps a well-ordered crystalline structure,[44,62] and the ringlike diffraction pattern of spots means structure distortion occurs after doping.[41]

4. APPLICATIONS

4.1. Electrocatalyst for Fuel Cell Application. A fuel cell is an electrochemical energy conversion device that oxidizes fuel at the anode and reduces oxygen from air at the cathode to produce electricity.[90] Commonly, Pt is used as the catalyst for the oxidation reaction on the anode and reduction reaction on cathode. However, the commercial application of Pt catalysts is limited by its scarcity, time-dependent drift, and CO poisoning.[90] Thus, Pt-based catalysts[91,92] and other metal catalysts, such as Au and Pd,[93,94] have been developed. Recently, N-graphene has been used in fuel cells as either the catalysts directly or carbon support to anchor metal catalysts.

4.1.1. Theoretical Part. The oxygen reduction reaction of N-graphene on the cathode of a fuel cell has been discussed in many studies. Through studying the ORR behavior of model graphenes $C_{45}NH_{20}$ and $C_{45}NH_{18}$ in acidic environment, Zhang et al.[25] showed that the spin density and charge density of atoms were the major factors that determined the catalytic active sites in ORR. The substitution of N atoms, which introduces the unpaired electron, will change the atomic charge distribution. The active sites in N-graphene usually are carbon atoms that possess high spin density. If the spin density is negative and small, the atom with a higher charge density will be the active sites. Although in a previous study,[95] it was shown that the energy gap between highest occupied molecular orbital (HOMO) and lowest unoccupied molecular orbital (LUMO) could be used as an index of kinetic stability, it is unnecessarily related to the catalytic capacity of graphene and N-graphene.

The ORR mechanism on N-graphene also has been studied. Earlier studies have shown that O_2 could be reduced following two pathways. One is a direct four-electron pathway in which O_2 is reduced to water in an acidic environment or OH^- in an alkaline environment. Another is a two-electron pathway in which O_2 is partly reduced to H_2O_2 in an acidic environment or OOH^- in an alkaline environment. Both mechanisms have been proposed by theoretical studies based on different N-graphene models. Kurak et al.[96] showed a two-electron ORR pathway based on the graphene model possessing two neighbor

dx.doi.org/10.1021/cs200652y | ACS Catal. 2012, 2, 781−794

N atoms in the zigzag edge. However, it was found that two nitrogen atoms were very unlikely to be doped at two neighboring zigzag sites by checking the interaction energy between two nitrogen atoms.[97]

Zhang et al.[25] proposed a four-electron ORR pathway on N-graphene in an acidic environment. Furthermore, after taking the solvent, surface coverage, and adsorbates into consideration, Yu et al.[98] obtained the overall energy profile of the ORR pathway on N-graphene in an alkaline environment. The study shows that water molecules are essential for the reaction. The O_2 adsorption is greatly enhanced due to the O_2 polarization induced by the hydrogen bonding with water. Through investigating two ORR mechanisms, dissociative and associative (Figure 11), study shows that the associative mechanism is

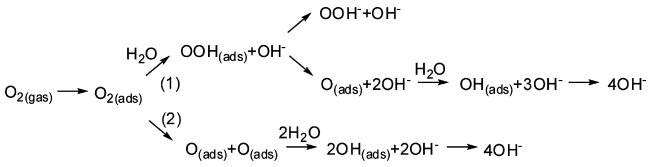

Figure 11. Scheme of the ORR reaction on N-graphene in an alkaline environment where 1 is the associative mechanism and 2 is the dissociative mechanism.[98]

more energetically favored in ORR because of the lower O_2 dissociation barrier. In the associative mechanism, the desorption barrier of $OOH_{(ads)}$ into OOH^- is high, so the energetically favored reaction $OOH_{(ads)} \rightarrow O_{(ads)} + OH^-$ is more likely to happen, which suggests the four-electron ORR pathway of N-graphene. The reaction rate is determined by the removal of $O_{(ads)}$ on the surface of N-graphene.

Apart from N-graphene, the interaction between Pt atom and N-graphene has been investigated.[26] In N-graphene, the nitrogen atoms do not bond with Pt atom directly; instead, they direct a Pt atom to bond with the carbon atom, which is more energetically favored. This is helpful to prevent Pt nanoclusters from migrating and forming larger particles. Because the introduction of nitrogen atoms disrupts the delocalized double bond in the graphene system, the Pt/C bond will focus on the 6s/2s orbitals rather than 5d/2p orbitals. This doubles the binding energy between Pt and carbon atoms. In general, the binding of Pt to N-graphene improves the catalytic durability of Pt.

4.1.2. Experimental Part. Several groups have recently reported studies on metal-free N-graphene with enhanced catalytic activity toward ORR.[23,40,41,52,60,62] The efficiency of ORR can be evaluated through two ways.[99] One way is to calculate the transfer number of electrons through the Koutecky–Levich (K–L) equation by using a rotating disk electrode (RDE). Another way is to measure the proportion of H_2O_2 formed during the ORR process by using a rotating ring-disk electrode. Qu et al.[41] reported that N-graphene exhibited a typical one-step, four-electron ORR pathway, which is similar to the ORR pathway of a Pt catalyst (Figure 12a). In contrast, pristine graphene showed a two-step, two-electron ORR pathway with a lower onset potential. In another work,[60] the H_2O_2 formed in the ORR process was about 10% at −0.5 V in the diffusion-controlled region. The low proportion of H_2O_2 indicated the four electron reduction process dominated in ORR. All these studies show that N-graphene can be a very effective catalyst for ORR.

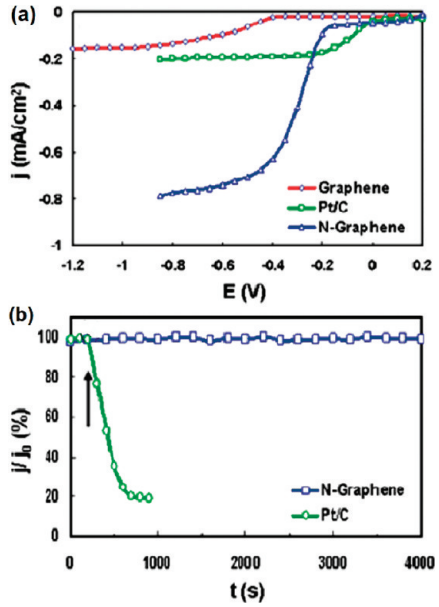

Figure 12. (a) RRDE voltammograms for ORR in air-saturated 0.1 M KOH on the electrodes graphene (red), Pt/C (green), and N-graphene (blue) with a scan rate of 0.01 V s^{-1}. Electrode rotating rate: 1000 rpm. (b) Current–time chronoamperometric response of Pt/C and NG to CO. The arrow indicates the addition of 10% (v/v) CO at −0.4 V.[41]

Furthermore, the ORR activity of N-graphene is also studied through diffusion limited current and kinetic current. Some studies showed the diffusion-limited current density of N-graphene was higher than commercial 20% or 40% Pt/C (E-TEK) catalyst,[41,52] but another study showed that N-graphene had a similar diffusion-limited current density.[60] Although the reported activity of N-graphene varies from different studies, there is consensus that N-graphene has excellent stability compared with the Pt catalyst. Shao et al.[23] reported that the 20% Pt/C (E-TEK) showed higher electrocatalytic activity than N-graphene before an accelerated degradation test (ADT), but after the ADT, the N-graphene exhibited higher kinetic current compared with the Pt/C catalyst because of the degradation of Pt/C. In addition, studies also showed the activity of N-graphene would not be influenced by the addition of methanol or CO (Figure 12b).[23,41] These two advantages make N-graphene a promising material toward ORR in fuel cells.

Notably, in the above studies in which the four-electron ORR pathway was observed, these N-graphene catalysts consist of two or three nitrogen types.[23,41,52,60,62] For N-graphene possessing only the pyridinic N, a two-electron reduction process was observed in the ORR process.[40] This may indicate a less efficient ORR performance of pyridinic N. In another study, the N-graphene with higher pyridinic and quaternary N content exhibited a higher onset potential than N-graphene that possessed the same nitrogen content. This suggests the pyridinic and quaternary N may play a more important role for ORR activity.[60] However, because of the scarcity of study in this field and variation in experimental conditions, the relationship between the catalytic activity and the nitrogen species is still unclear. In the former study of N-CNTs, both quaternary[100,101] and pyridinic[21,24] nitrogen have been observed to have the dominant effect for the ORR activity. Thus, further research work on the nitrogen catalytic site is still required.

dx.doi.org/10.1021/cs200652y | ACS Catal. 2012, 2, 781–794

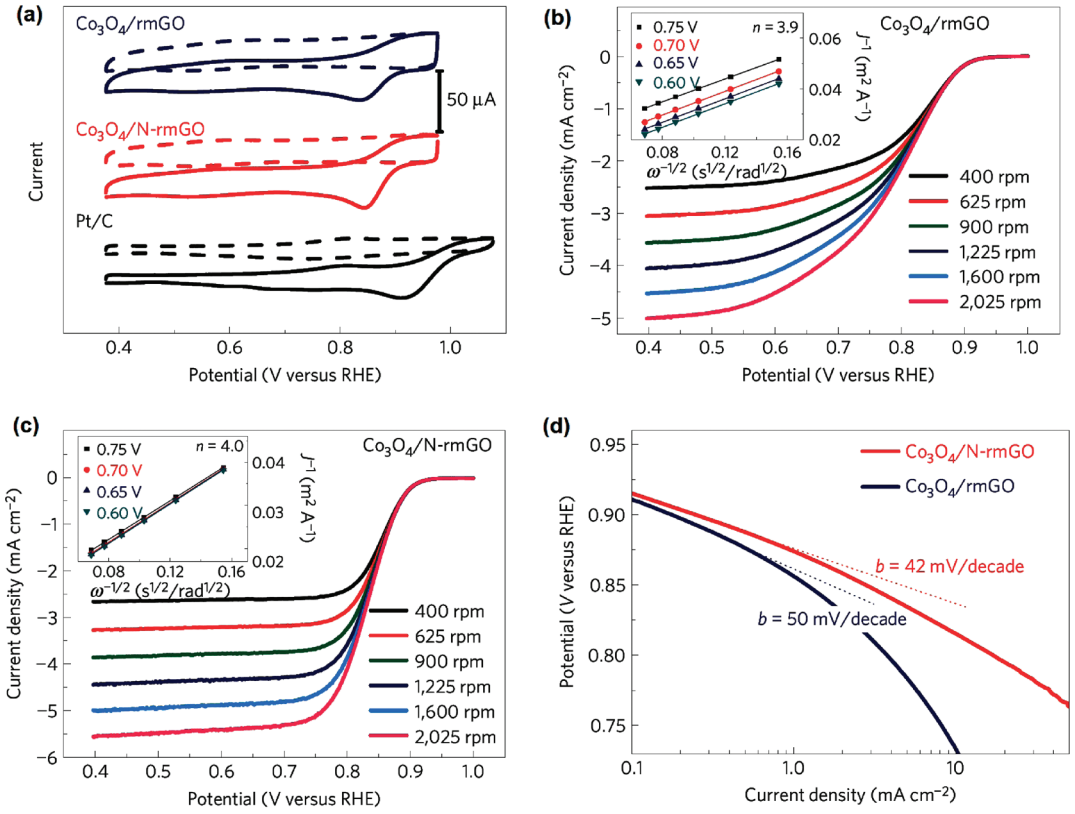

Figure 13. (a) Cyclic voltammetry (CV) of Co_3O_4/rmGO, Co_3O_4/N-rmGO and Pt/C in O_2- (solid line) or Ar-saturated (dashed line) 0.1 M KOH solution. RDE voltammograms of Co_3O_4/rmGO (b) and Co_3O_4/N-rmGO (c) for ORR in O_2-saturated 0.1 M KOH at different rotation rates with a scan rate of 5 mV s^{-1}. The inset figure is the corresponding Koutecky–Levich plots at different potentials. (d) Tafel plots of Co_3O_4/rmGO and Co_3O_4/N-rmGO derived by the mass-transport correction.[104]

Apart from the nitrogen types, the nitrogen content is also related to the ORR activity of N-graphene. However, because N-graphene usually consists of two or three nitrogen types and the content of different nitrogen types usually varies with different nitrogen doping levels, different studies have produced contradictory results in previous studies.[52,62] In a more direct study in which N-graphene contains only pyridinic N,[40] the N-graphene possessing the higher nitrogen content (16 at. %) exhibited poorer ORR activity than that possessing the lower nitrogen content (2.2 at. %). In a theoretical study, it has been reported that model graphene with a higher nitrogen content was more easily poisoned by $O_{(ads)}$ because of the stronger affinity.[102] These results mean an optimal nitrogen content might be critical to achieving a high ORR activity.

Several studies also have studied the performance of Pt/N-graphene in both oxidation and reduction reactions.[67,73] For Pt/N-graphene used for an oxidation reaction,[73] it has been reported that Pt nanoparticles could disperse better on the surface of N-graphene with the existence of N atoms in a carbon lattice. Moreover, the conductivity of N-graphene was improved at high temperature (800 °C). These two factors made Pt/N-graphene exhibit a 3 times higher oxidation current than 20% Pt/carbon black catalyst. For Pt/N-graphene used for the oxygen reduction reaction,[67] it also showed an improved performance compared with Pt/graphene because of the better dispersion of Pt nanoparticles and stronger interaction between Pt and C atoms stated in the theoretical part.[26]

Apart from the Pt catalyst, other nonprecious metal catalysts supported on N-graphene toward ORR have been studied.[103,104] Tsai et al.[103] synthesized FeCN/N-graphene by impregnating N-graphene into a mixture of iron acetate and 1,10-phenanthroline, then the Fe_xC species formed in the sintering process would anchor the FeCN nanoparticles on N-graphene surface. The as-synthesized FeCN/N-graphene shows an enhanced ORR activity compared with the N-graphene because of the additional ORR activity of FeCN nanoparticles. In another notable study,[104] Liang et al. grew Co_3O_4 on mildly oxidized graphene oxide (rmGO) with or without the presence of NH_4OH, then catalyst Co_3O_4/rmGO and Co_3O_4/N-rmGO were obtained. The latter catalyst has ~4 at. % nitrogen content. Through the ORR study of the Co_3O_4/rmGO and Co_3O_4/N-rmGO, it has been revealed that these two catalysts exhibit high ORR activity that is different from the Co_3O_4 nanocrystals (Figure 13a). Also different from the two-electron ORR pathway of N-rmGO obtained in the study, these two catalysts show the obvious four-electron ORR pathway (Figure 13b, c). Comparing the kinetic current of Co_3O_4/N-rmGO with Co_3O_4/rmGO, the former exhibits the apparent higher current density than the latter (Figure 13d). The higher ORR activity of Co_3O_4/N-rmGO is ascribed to the synergistic coupling between Co_3O_4 and N-graphene. Because Co_3O_4/N-rmGO shows both the high ORR activity similar to Pt catalyst and excellent stability, this kind of hybrid catalyst is also promising for ORR catalysis.

4.2. Field-Effect Transistor (FET). For semiconductors, the flow of electricity needs some kind of activation (for example, heat or light absorption) to get over the gap between the valence band and conduction band.[105] If the semiconductor is activated by the external electric field to switch "on" and "off", then it is called FET. Generally speaking, the large-scale and

dx.doi.org/10.1021/cs200652y | ACS Catal. 2012, 2, 781–794

bilayer graphene do not possess a band gap; however, constraining large-scale graphene in one dimension (GNRs) or applying an electric field perpendicularly on the bilayer graphene can induce the band gap (Figure 14).[106] Recently, both theoretical and experimental works have studied the semiconductor properties of N-graphene.

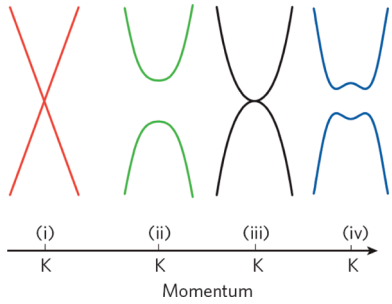

Figure 14. Band structure around the k point of (i) large-area graphene, (ii) graphene nanoribbons, (iii) unbiased bilayer graphene, and (iv) bilayer graphene with an applied perpendicular field.[106]

4.2.1. Theoretical Part. Nitrogen doping can effectively modulate the electrical properties of graphene. On the basis of the investigation of C_3N_4 and $C_6N_9H_3$ graphene,[29] it has been revealed that the band gap of N-graphene with a high N/C ratio reached ~5 eV. The band gap can be tuned by the presence of external stress or adatoms. In another theoretical work based on the study of delta-doping graphene,[107] it has been reported that the band gap could be opened only when the nitrogen content was over ~25%. However, delta-doping may be unlikely to occur in practice. In the experimental study, an obvious band gap has been observed on N-graphene with a lower nitrogen content.[70] Apart from the band gap, the mobility and conductivity of N-graphene has also been discussed theoretically by using the quantum-mechanical Kubo-Greenwood approach.[27] When the nitrogen concentration (C_d) is over or equal to 2% ($2\% \leq C_d \leq 4\%$), the decay of the diffusion coefficient D is clearly observed. This indicates the onset of quantum interference effects. However, this effect is still weak and can only marginally affect the conduction when the nitrogen content is low. This study suggests that the nitrogen doping may modulate the graphene property while maintaining good mobility and conductivity. However, the conduction is also influenced by many other factors. In experimental study, it has been shown that both defects and nitrogen atoms will be introduced into graphene. Defects can serve as the scattering center, which will affect the mobility of N-graphene. Moreover, when the nitrogen concentration rises over 5%, a stronger localization effect might occur, which will largely decrease the mobility in N-graphene.[27]

GNR can be obtained by constraining large-scale graphene to one dimension. Former studies have revealed that H-terminated GNRs with either armchair or zigzag-shaped edges have nonzero band gaps.[7,9,108] Through theoretical studies of zigzag GNR (ZGNR),[109,110] it was revealed that the nitrogen atom and defects energetically preferred to dope at the edge of GNR. Depending on doping sites and various GNRs, the introduction of nitrogen atoms will induce very different electronic properties. For example, Yu et al.[109] showed different nitrogen doping sites would make the impurity state lie below or above the Fermi level. Li et al.[110] found one edge-doped nitrogen made ZGNR spin a gapless semiconductor while two opposite edge-doped nitrogens made ZGNR nonmagnetic metals. Biel et al.[111] reported that the full suppression of impurity backscattering would occur if the doped GNR was armchair and mirror-symmetrical.

4.2.2. Experimental Part. After the preparation of bottom-gated N-graphene FET by using a Si substrate with a 500 nm thick SiO_2 layer (Figure 15a), pristine graphene exhibits p-type behavior because of the adsorption of oxygen or water in air (Figure 15b). In contrast, N-graphene with a 8.9 at. % nitrogen

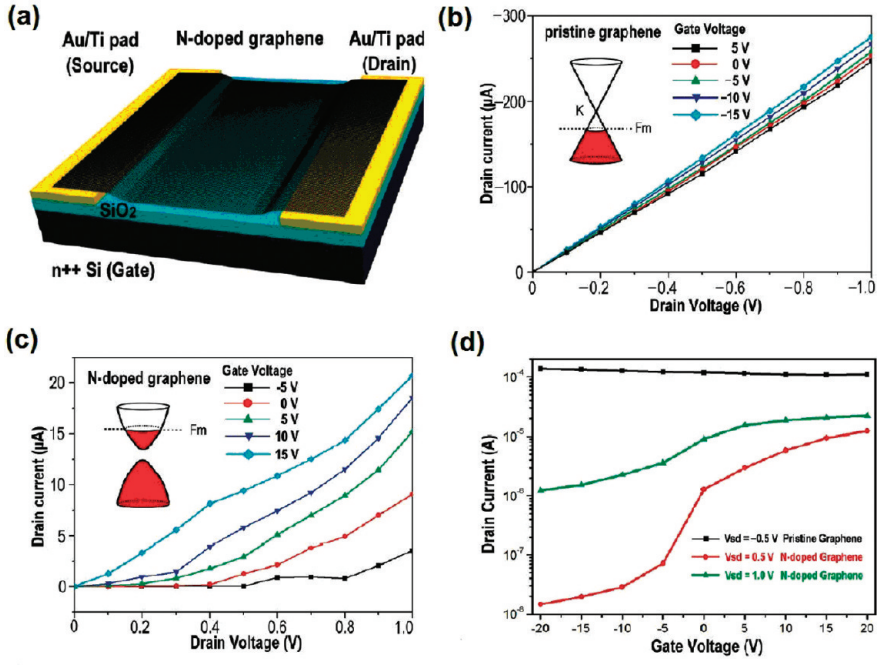

Figure 15. (a) Schematic illustration of the N-graphene FET device. (b, c) I_{ds}/V_{ds} characteristics at various V_g's for the pristine graphene and NG FET device. (d) Transfer characteristics of the pristine graphene and the NG.[30]

dx.doi.org/10.1021/cs200652y | ACS Catal. 2012, 2, 781–794

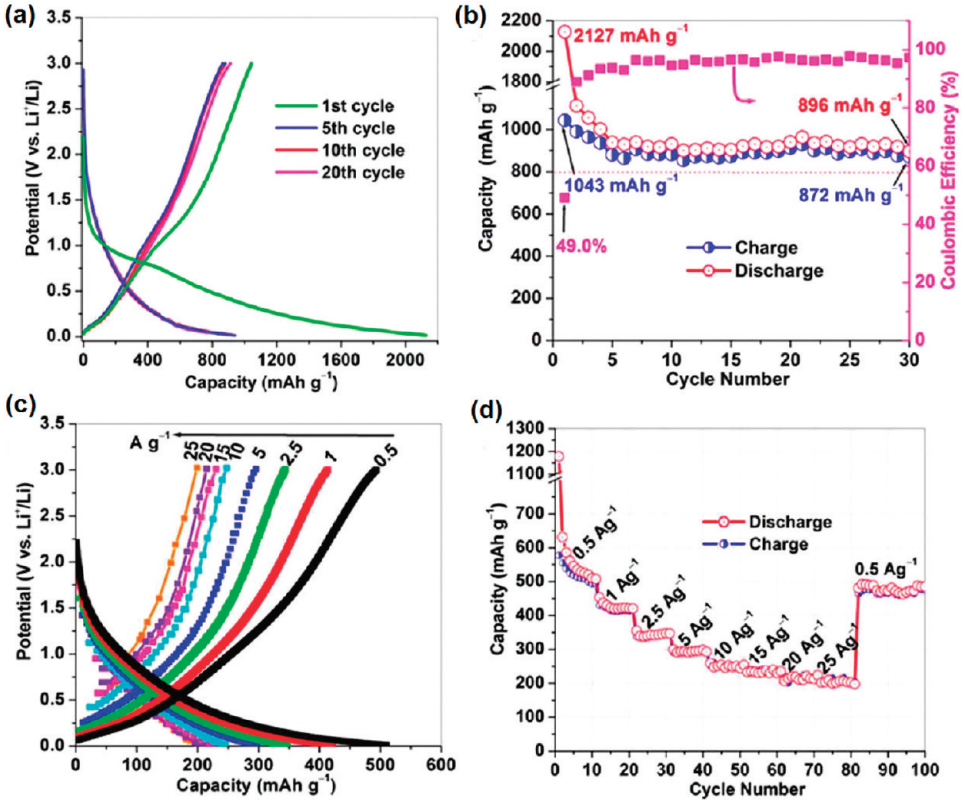

Figure 16. Galvanostatic charge−discharge profile of N-graphene at a low current rate of 50 mA/g (a) and a higher current rate from 0.5 to 25 A/g (c), (b) cycle performance and Coulombic efficiency of N-graphene at low current rate of 50 mA/g, (d) cycle performance and rate capabilities of N-graphene at higher current rate from 0.5 to 25 A/g.[115]

doping level exhibits typical n-type semiconductor behavior (Figure 15c, d).[30] Compared with the mobility of pristine graphene (300−1200 $cm^2 V^{-1} s^{-1}$), the mobility of N-graphene reduces to 200−450 $cm^2 V^{-1} s^{-1}$. Using different precursors in the CVD method, Jin et al.[44] reported the mobility of N-graphene with 2.4 at. % nitrogen content reduced by 2 orders of magnitude compared with that of pristine graphene. In other methods,[50,59,63] such as N-graphene obtained through NH_3 annealing after N^+ ion irradiation,[59] a much lower hole and electron conductivity was observed compared with the pristine graphene.

In the study of nitrogen-doped GNR (N-GNR), it has been reported the N-GNR fabricated by high power electrical annealing in NH_3 showed typical n-type semiconductor behavior, and the mobility was similar with the GNR annealed in vacuum.[31] The reason is that nitrogen atoms incorporate mainly into the edge of GNR, and few charged impurities are introduced, which will not degrade the mobility of GNR.

As discussed above, the electron mobility of graphene decreases with the increment of band gap in most cases, which is similar to the trend in studies of CNTs.[106,112,113] Although several theoretical studies[27,111] and the recent work about N-GNR[31] have shown the mobility of N-graphene might be maintained by controlling the nitrogen at a low doping level and specific doping site, the scattering center induced by the defects will drastically decrease the mobility of N-graphene in practice. In addition, it is claimed that the grain boundaries in N-graphene may also contribute to a decrement of mobility.[36]

Other than the mobility, a sizable band gap, preferably 0.4 eV or higher, is also required in conventional FET (the band gap of silicon is 1.1 eV).[106] Until now, only a few studies of N-graphene have reported a band gap in their works. Zhang et al. showed the band gap in N-graphene with 2.9 at. % nitrogen content was about 0.16 eV,[50] which is still too low. Considering the mobility and band gap of N-graphene obtained up to the present, synthesization of N-graphene for practical applications is still far off.

4.3. Lithium Ion Batteries. In recently years, graphene has attracted great attention as a potential anode material in lithium ion batteries (LIBs) because of its fascinating properties, such as high electrical electronic properties, high surface area, and excellent mechanical flexibility. Although graphene-based materials can reach a high reversible capacity (1013−1054 mA h/g) at a low charge rate,[114] it is still rate-limited at a high charge/discharge rate (≥500 mA/g).[115] Thus, a N-graphene-based device is proposed with the intent to achieve a high reversible capacity at the high charge/discharge rate.

In earlier work, Reddy et al.[43] obtained N-doped graphene under the control of a CVD method. The reversible discharge capacity of N-graphene was almost double compared with pristine graphene because of the enhanced Li ion intercalation with the introduction of nitrogen atoms. In another more recent work,[116] N-GNS with 2 at. % nitrogen content (57.4% pyridinic, 35.0% pyrrolic, and 7.6% quaternary N) was synthesized by heat treatment of GO in an NH_3 atmosphere. The N-graphene possessed a reversible capacity of around 900 mA h/g at a current density of 42 mA/g and a capacity of ~250 mA h g^{-1} at a high current density of 2.1 A/g. In another work in which N-graphene was synthesized by a similar heat treatment method,[115] N-graphene with 3.13 at. % nitrogen content exhibited reversible capacities of 1043 mAh/g and 872 mAh/g in the first and 31st cycles at a low current rate of 50

dx.doi.org/10.1021/cs200652y | ACS Catal. 2012, 2, 781−794

mA/g, respectively (Figure 16 a, b). At a higher current rate of 25 A/g, the reversible capacities of N-graphene still reached 199 mAh/g (Figure 16 c, d).

The excellent performance of N-graphene can be ascribed to many factors, such as the introduction of nitrogen atoms, the defects and disordered surface morphology induced by doping, increased electrode/electrolyte wettability, and improved electrochemical performance. Notably, in the above studies, the types of pyridinic and pyrrolic N are predominant in the N-graphene. Through the study of nitrogen-doped graphite, it has been revealed that both the pyridinic and quaternary N played an effective role in lithium intercalation and extraction.[117] Thus, graphene with a large quaternary N content might also be used in LIBs.

4.4. Devices in Other Fields. N-Graphene has been applied in the field of ultracapacitors.[69] The ultracapacitor based on N-graphene has shown a long cycle life (Figure 17a).

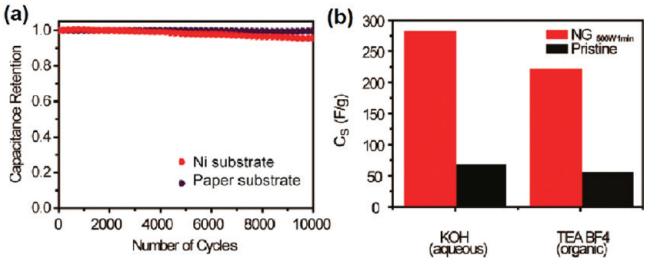

Figure 17. (a) The cycling tests for the ultracapacitors based on Ni and paper substrates up to 10 000 cycles. (b) The specific capacitances measured in 6 M KOH and organic electrolytes.[69]

Moreover, a N-graphene-based device showed a much higher capacitance than a device based on pristine graphene in both KOH and organic electrolyte (Figure 17b). By calculating the binding energy between the potassium ion and nitrogen configurations at different positions of N-graphene, it has been revealed that the basal-plane pyridinic N exhibited the largest binding energy. Thus, basal-plane pyridinic N was claimed to have a dominant role in the capacitance enhancement. Pyrrolic N also showed a large binding energy with ion, but the negative charge of pyrrolic N would cause too strong binding for the reversible charging/discharging process, which was reflected by the lower Coulombic efficiencies of N-graphene with a large proportion of pyrrolic N. Therefore, controlling the appropriate nitrogen configuration can greatly promote the capacitance of N-graphene.

Study has shown that N-graphene has a better electron transfer efficiency than pristine graphene,[68,72] rendering its potential use for electrochemical sensing. Because glucose oxidase (GO_x) could oxidize glucose with oxygen and produce gluconic acid and H_2O_2, Wang et al.[68] fabricated the glucose sensor by immobilizing GO_x on the biocompatible N-graphene surface. It was observed that the GO_x redox peak current on N-doped graphene was greatly improved over that on graphene, which demonstrated the enhanced electron transfer efficiency of N-graphene. This kind of biosensor shows a good response for glucose concentrations ranging from 0.01 to 0.5 mM in the presence of other molecules.

Apart from the above applications, N-graphene also has been used as a support to anchor quantum dots toward high-performance photocatalysts.[118] N-Graphene/CdS nanocomposites have a higher photocatalytic activity than graphene/CdS and pure CdS, which can be attributed to the hampering of the radiative recombination of the electron−hole pairs induced by enhanced electron transportation from CdS to N-graphene. Moreover, CdS anchored on N-graphene with 2 wt % nitrogen content showed the best catalytic activity. It reveals that a proper junction structure is required for the highest photocatalytic activity.

5. CONCLUSION

In summary, many research works on N-graphene have emerged in recent years. Various synthesis approaches and characterization techniques have been explored to obtain and characterize N-graphene. The N doping offers an effective way to tailor the properties of graphene, thus making N-graphene a promising material for use in many fields. However, the method for the production of large-scale N-graphene is still lacking; thus, new methods are required. Moreover, synthesizing N-graphene meets problems similar to those encountered during fabricating N-CNT. First, controlling the nitrogen type and distribution is unresolved. Second, to achieve nitrogen doping at specific positions and with precise control of doping content is still a challenge. For FET application, the doping location and doping content is critical not to decrease the electron mobility drastically while opening a suitable band gap. For electrocatalysis, the correlation between the activity and nitrogen type needs to be identified, and controlling the specific nitrogen type in N-graphene is required for high performance catalysts. For other applications, such as LIBs and ultracapacitors, a specific nitrogen type may also be required. Another issue to be considered is defects and distortion. Defects are inevitable during the synthesis process of N-graphene. They will decrease the mobility of N-graphene; however, their presence will benefit the catalytic reaction for ORR and LIBs. Depending on the application, choosing or finding an appropriate approach is required.

AUTHOR INFORMATION

Corresponding Author

*Phone: (65) 6316 8866. Fax: (65) 6794 7553. E-mail: WangXin@ntu.edu.sg.

Notes

The authors declare no competing financial interest.

ACKNOWLEDGMENTS

This work is supported by the academic research fund AcRF tier 2 (MOE2009-T2-2-024), Ministry of Education, Singapore, and competitive research program (2009 NRF-CRP 001-032), National Research Foundation, Singapore.

REFERENCES

(1) Novoselov, K. S.; Geim, A. K.; Morozov, S. V.; Jiang, D.; Zhang, Y.; Dubonos, S. V.; Grigorieva, I. V.; Firsov, A. A. *Science* **2004**, *306*, 666.
(2) Stoller, M. D.; Park, S.; Zhu, Y.; An, J.; Ruoff, R. S. *Nano Lett.* **2008**, *8*, 3498.
(3) Balandin, A. A.; Ghosh, S.; Bao, W.; Calizo, I.; Teweldebrhan, D.; Miao, F.; Lau, C. N. *Nano Lett.* **2008**, *8*, 902.
(4) Lee, C.; Wei, X.; Kysar, J. W.; Hone, J. *Science* **2008**, *321*, 385.
(5) Barone, V.; Hod, O.; Scuseria, G. E. *Nano Lett.* **2006**, *6*, 2748.
(6) Kosynkin, D. V.; Higginbotham, A. L.; Sinitskii, A.; Lomeda, J. R.; Dimiev, A.; Price, B. K.; Tour, J. M. *Nature* **2009**, *458*, 872.
(7) Li, X.; Wang, X.; Zhang, L.; Lee, S.; Dai, H. *Science* **2008**, *319*, 1229.

(8) Ponomarenko, L. A.; Schedin, F.; Katsnelson, M. I.; Yang, R.; Hill, E. W.; Novoselov, K. S.; Geim, A. K. *Science* **2008**, *320*, 356.
(9) Ritter, K. A.; Lyding, J. W. *Nat. Mater.* **2009**, *8*, 235.
(10) Jiao, L.; Zhang, L.; Wang, X.; Diankov, G.; Dai, H. *Nature* **2009**, *458*, 877.
(11) Derycke, V.; Martel, R.; Appenzeller, J.; Avouris, P. *Appl. Phys. Lett.* **2002**, *80*, 2773.
(12) Gong, K.; Du, F.; Xia, Z.; Durstock, M.; Dai, L. *Science* **2009**, *323*, 760.
(13) Wang, S. Y.; Wang, X.; Jiang, S. P. *Langmuir* **2008**, *24*, 10505.
(14) Wang, S. Y.; Yang, F.; Chen, S. L.; Jiang, S. P.; Wang, X. *Electrochem. Commun.* **2010**, *12*, 1646.
(15) Zhou, C.; Kong, J.; Yenilmez, E.; Dai, H. *Science* **2000**, *290*, 1552.
(16) Schedin, F.; Geim, A. K.; Morozov, S. V.; Hill, E. W.; Blake, P.; Katsnelson, M. I.; Novoselov, K. S. *Nat. Mater.* **2007**, *6*, 652.
(17) Giovannetti, G.; Khomyakov, P. A.; Brocks, G.; Karpan, V. M.; van den Brink, J.; Kelly, P. J. *Phys. Rev. Lett.* **2008**, *101*, 026803.
(18) Chen, W.; Chen, S.; Qi, D. C.; Gao, X. Y.; Wee, A. T. S. *J. Am. Chem. Soc.* **2007**, *129*, 10418.
(19) Ewels, C. P.; Glerup, M. *J. Nanosci. Nanotechnol.* **2005**, *5*, 1345.
(20) Casanovas, J.; Ricart, J. M.; Rubio, J.; Illas, F.; Jiménez-Mateos, J. M. *J. Am. Chem. Soc.* **1996**, *118*, 8071.
(21) Kundu, S.; Nagaiah, T. C.; Xia, W.; Wang, Y.; Dommele, S. V.; Bitter, J. H.; Santa, M.; Grundmeier, G.; Bron, M.; Schuhmann, W.; Muhler, M. *J. Phys. Chem. C* **2009**, *113*, 14302.
(22) Matter, P. H.; Zhang, L.; Ozkan, U. S. *J. Catal.* **2006**, *239*, 83.
(23) Shao, Y.; Zhang, S.; Engelhard, M. H.; Li, G.; Shao, G.; Wang, Y.; Liu, J.; Aksay, I. A.; Lin, Y. *J. Mater. Chem.* **2010**, *20*, 7491.
(24) Biddinger, E. J.; Deak, D. V.; Ozkan, U. S. *Top. Catal.* **2009**, *52*, 1566.
(25) Zhang, L. P.; Xia, Z. H. *J. Phys. Chem. C* **2011**, *115*, 11170.
(26) Groves, M. N.; Chan, A. S. W.; Malardier-Jugroot, C.; Jugroot, M. *Chem. Phys. Lett.* **2009**, *481*, 214.
(27) Lherbier, A.; Blase, X.; Niquet, Y. M.; Triozon, F.; Roche, S. *Phys. Rev. Lett.* **2008**, *101*, 036808.
(28) Wu, M.; Cao, C.; Jiang, J. Z. *Nanotechnology* **2010**, *21*, 505202.
(29) Deifallah, M.; McMillan, P. F.; Corà, F. *J. Phys. Chem. C* **2008**, *112*, 5447.
(30) Wei, D.; Liu, Y.; Wang, Y.; Zhang, H.; Huang, L.; Yu, G. *Nano Lett.* **2009**, *9*, 1752.
(31) Wang, X.; Li, X.; Zhang, L.; Yoon, Y.; Weber, P. K.; Wang, H.; Guo, J.; Dai, H. *Science* **2009**, *324*, 768.
(32) Huang, X.; Yin, Z.; Wu, S.; Qi, X.; He, Q.; Zhang, Q.; Yan, Q; Boey, F.; Zhang, H. *Small* **2011**, *7*, 1876.
(33) Guo, S.; Dong, S. *Chem. Soc. Rev.* **2011**, *40*, 2644.
(34) Wei, D.; Liu, Y. *Adv. Mater.* **2010**, *22*, 3225.
(35) Liu, H.; Liu, Y.; Zhu, D. *J. Mater. Chem.* **2011**, *21*, 3335.
(36) Reina, A.; Jia, X. T.; Ho, J.; Nezich, D.; Son, H.; Bulovic, V.; Dresselhaus, M. S.; Kong, J. *Nano Lett.* **2009**, *9*, 30.
(37) Zhang, J.; Zou, H.; Qing, Q.; Yang, Y.; Li, Q.; Liu, Z.; Guo, X.; Du, Z. *J. Phys. Chem. B* **2003**, *107*, 3712.
(38) Che, G.; Lakshmi, B. B.; Martin, C. R.; Fisher, E. R.; Ruoff, R. S. *Chem. Mater.* **1998**, *10*, 260.
(39) Maldonado, S.; Morin, S.; Stevenson, K. J. *Carbon* **2006**, *44*, 1429.
(40) Luo, Z.; Lim, S.; Tian, Z.; Shang, J.; Lai, L.; MacDonald, B.; Fu, C.; Shen, Z.; Yu, T.; Lin, J. *J. Mater. Chem.* **2011**, *21*, 8038.
(41) Qu, L.; Liu, Y.; Baek, J. B.; Dai, L. *ACS Nano* **2010**, *4*, 1321.
(42) Di, C. A.; Wei, D.; Yu, G.; Liu, Y.; Guo, Y.; Zhu, D. *Adv. Mater.* **2008**, *20*, 3289.
(43) Reddy, A. L. M.; Srivastava, A.; Gowda, S. R.; Gullapalli, H.; Dubey, M.; Ajayan, P. M. *ACS Nano* **2010**, *4*, 6337.
(44) Jin, Z.; Yao, J.; Kittrell, C.; Tour, J. M. *ACS Nano* **2011**, *5*, 4112.
(45) Imamura, G.; Saiki, K. *J. Phys. Chem. C* **2011**, *115*, 10000.
(46) Cho, Y. J.; Kim, H. S.; Baik, S. Y.; Myung, Y.; Jung, C. S.; Kim, C. H.; Park, J.; Kang, H. S. *J. Phys. Chem. C* **2011**, *115*, 3737.
(47) Kudashov, A. G.; Okotrub, A. V.; Bulusheva, L. G.; Asanov, I. P.; Shubin, Y. V.; Yudanov, N. F.; Yudanova, L. I.; Danilovich, V. S.; Abrosimov, O. G. *J. Phys. Chem. B* **2004**, *108*, 9048.
(48) Liu, J.; Webster, S.; Carroll, D. L. *J. Phys. Chem. B* **2005**, *109*, 15769.
(49) Lv, W. X.; Zhang, R.; Xia, T. L.; Bi, H. M.; Shi, K. Y. *J. Nanopart. Res.* **2011**, *13*, 2351.
(50) Zhang, C.; Fu, L.; Liu, N.; Liu, M.; Wang, Y.; Liu, Z. *Adv. Mater.* **2011**, *23*, 1020.
(51) Choucair, M.; Thordarson, P.; Stride, J. A. *Nat. Nanotechnol.* **2009**, *4*, 30.
(52) Deng, D.; Pan, X.; Yu, L.; Cui, Y.; Jiang, Y.; Qi, J.; Li, W. X.; Fu, Q.; Ma, X.; Xue, Q.; Sun, G.; Bao, X. *Chem. Mater.* **2011**, *23*, 1188.
(53) Droppa, R.; Hammer, P.; Carvalho, A. C. M.; dos Santos, M. C.; Alvarez, F. *J. Non-Cryst. Solids* **2002**, *299−302*, 874.
(54) Journet, C.; Maser, W. K.; Bernier, P.; Loiseau, A.; Lamy de la Chapelle, M.; Lefrant, S.; Deniard, P.; Lee, R.; Fischer, J. E. *Nature* **1997**, *388*, 756.
(55) Suenaga, K.; Colliex, C.; Demoncy, N.; Loiseau, A.; Pascard, H.; Willaime, F. *Science* **1997**, *278*, 653.
(56) Panchakarla, L. S.; Subrahmanyam, K. S.; Saha, S. K.; Govindaraj, A.; Krishnamurthy, H. R.; Waghmare, U. V.; Rao, C. N. R. *Adv. Mater.* **2009**, *21*, 4726.
(57) Ghosh, A.; Late, D. J.; Panchakarla, L. S.; Govindaraj, A.; Rao, C. N. R. *J. Exp. Nanosci.* **2009**, *4*, 313.
(58) Subrahmanyam, K. S.; Panchakarla, L. S.; Govindaraj, A.; Rao, C. N. R. *J. Phys. Chem. C* **2009**, *113*, 4257.
(59) Guo, B.; Liu, Q.; Chen, E.; Zhu, H.; Fang, L.; Gong, J. R. *Nano Lett.* **2010**, *10*, 4975.
(60) Geng, D.; Chen, Y.; Chen, Y.; Li, Y.; Li, R.; Sun, X.; Ye, S.; Knights, S. *Energy Environ. Sci.* **2011**, *4*, 760.
(61) Kinoshita, K. *Carbon: Electrochemical and Physicochemical Properties*; Wiley: New York, 1988.
(62) Sheng, Z. H.; Shao, L.; Chen, J. J.; Bao, W. J.; Wang, F. B.; Xia, X. H. *ACS Nano* **2011**, *5*, 4350.
(63) Li, X.; Wang, H.; Robinson, J. T.; Sanchez, H.; Diankov, G.; Dai, H. *J. Am. Chem. Soc.* **2009**, *131*, 15939.
(64) Golberg, D.; Bando, Y.; Bourgeois, L.; Kurashima, K.; Sato, T. *Carbon* **2000**, *38*, 2017.
(65) Morant, C.; Andrey, J.; Prieto, P.; Mendiola, D.; Sanz, J. M.; Elizalde, E. *Phys. Status Solidi A* **2006**, *203*, 1069.
(66) Suenaga, K.; Johansson, M. P.; Hellgren, N.; Broitman, E.; Wallenberg, L. R.; Colliex, C.; Sundgren, J. E.; Hultman, L. *Chem. Phys. Lett.* **1999**, *300*, 695.
(67) Imran Jafri, R.; Rajalakshmi, N.; Ramaprabhu, S. *J. Mater. Chem.* **2010**, *20*, 7114.
(68) Wang, Y.; Shao, Y.; Matson, D. W.; Li, J.; Lin, Y. *ACS Nano* **2010**, *4*, 1790.
(69) Jeong, H. M.; Lee, J. W.; Shin, W. H.; Choi, Y. J.; Shin, H. J.; Kang, J. K.; Choi, J. W. *Nano Lett.* **2011**, *11*, 2472.
(70) Lin, Y. C.; Lin, C. Y.; Chiu, P. W. *Appl. Phys. Lett.* **2010**, *96*, 133110.
(71) Long, D.; Li, W.; Ling, L.; Miyawaki, J.; Mochida, I.; Yoon, S. H. *Langmuir* **2010**, *26*, 16096.
(72) Wang, D. W.; Gentle, I. R.; Lu, G. Q. *Electrochem. Commun.* **2010**, *12*, 1423.
(73) Zhang, L. S.; Liang, X. Q.; Song, W. G.; Wu, Z. Y. *Phys. Chem. Chem. Phys.* **2010**, *12*, 12055.
(74) Cançado, L. G.; Pimenta, M. A.; Neves, B. R. A.; Dantas, M. S. S.; Jorio, A. *Phys. Rev. Lett.* **2004**, *93*, 247401.
(75) Dresselhaus, M. S.; Dresselhaus, G.; Saito, R.; Jorio, A. *Phys. Rep.* **2005**, *409*, 47.
(76) Ferrari, A. C.; Meyer, J. C.; Scardaci, V.; Casiraghi, C.; Lazzeri, M.; Mauri, F.; Piscanec, S.; Jiang, D.; Novoselov, K. S.; Roth, S.; Geim, A. K. *Phys. Rev. Lett.* **2006**, *97*, 187401.
(77) Tuinstra, F.; Koenig, J. L. *J. Chem. Phys.* **1970**, *53*, 1126.
(78) Nemanich, R. J.; Solin, S. A. *Phys. Rev. B* **1979**, *20*, 392.

(79) Cançado, L. G.; Takai, K.; Enoki, T.; Endo, M.; Kim, Y. A.; Mizusaki, H.; Jorio, A.; Coelho, L. N.; Magalhães-Paniago, R.; Pimenta, M. A. *Appl. Phys. Lett.* **2006**, *88*, 163106.
(80) Das, A.; Pisana, S.; Chakraborty, B.; Piscanec, S.; Saha, S. K.; Waghmare, U. V.; Novoselov, K. S.; Krishnamurthy, H. R.; Geim, A. K.; Ferrari, A. C.; Sood, A. K. *Nat. Nanotechnol.* **2008**, *3*, 210.
(81) Ni, Z. H.; Wang, H. M.; Kasim, J.; Fan, H. M.; Yu, T.; Wu, Y. H.; Feng, Y. P.; Shen, Z. X. *Nano Lett.* **2007**, *7*, 2758.
(82) Graf, D.; Molitor, F.; Ensslin, K.; Stampfer, C.; Jungen, A.; Hierold, C.; Wirtz, L. *Nano Lett.* **2007**, *7*, 238.
(83) Wu, Y. H.; Yu, T.; Shen, Z. X. *J. Appl. Phys.* **2010**, *108*, 071301.
(84) Zhao, L.; He, R.; Rim, K. T.; Schiros, T.; Kim, K. S.; Zhou, H.; Gutiérrez, C.; Chockalingam, S. P.; Arguello, C. J.; Pálová, L.; Nordlund, D.; Hybertsen, M. S.; Reichman, D. R.; Heinz, T. F.; Kim, P.; Pinczuk, A.; Flynn, G. W.; Pasupathy, A. N. *Science* **2011**, *333*, 999.
(85) Casiraghi, C.; Pisana, S.; Novoselov, K. S.; Geim, A. K.; Ferrari, A. C. *Appl. Phys. Lett.* **2007**, *91*, 233108.
(86) Gupta, A.; Chen, G.; Joshi, P.; Tadigadapa, S.; Eklund, P. C. *Nano Lett.* **2006**, *6*, 2667.
(87) Ferrari, A. C. *Solid State Commun.* **2007**, *143*, 47.
(88) Herz, M.; Giessibl, F. J.; Mannhart, J. *Phys. Rev. B* **2003**, *68*, 045301.
(89) Zheng, B.; Hermet, P.; Henrard, L. *ACS Nano* **2010**, *4*, 4165.
(90) Yu, Y. L.; Hu, Y. P.; Liu, X.; Deng, W. Q.; Wang, X. *Electrochim. Acta* **2009**, *54*, 3092.
(91) Sun, S.; Murray, C. B.; Weller, D.; Folks, L.; Moser, A. *Science* **2000**, *287*, 1989.
(92) Kristian, N.; Yan, Y. S.; Wang, X *Chem. Commun.* **2008**, 353.
(93) Kristian, N.; Yu, Y. L.; Gunawan, P.; Xu, R.; Deng, W. Q.; Liu, X. W.; Wang, X. *Electrochim. Acta* **2009**, *54*, 4916.
(94) Wang, Y.; Nguyen, T.; Liu, X.; Wang, X. *J. Power Sources* **2010**, *195*, 2619.
(95) Aihara, J. I. *J. Phys. Chem. A* **1999**, *103*, 7487.
(96) Kurak, K. A.; Anderson, A. B. *J. Phys. Chem. C* **2009**, *113*, 6730.
(97) Huang, S. F.; Terakura, K.; Ozaki, T.; Ikeda, T.; Boero, M.; Oshima, M.; Ozaki, J. I.; Miyata, S. *Phys. Rev. B* **2009**, *80*, 235410.
(98) Yu, L.; Pan, X.; Cao, X.; Hu, P.; Bao, X. *J. Catal.* **2011**, *282*, 183.
(99) Paulus, U. A.; Schmidt, T. J.; Gasteiger, H. A.; Behm, R. J. *J. Electroanal. Chem.* **2001**, *495*, 134.
(100) Nagaiah, T. C.; Kundu, S.; Bron, M.; Muhler, M.; Schuhmann, W. *Electrochem. Commun.* **2010**, *12*, 338.
(101) Niwa, H.; Horiba, K.; Harada, Y.; Oshima, M.; Ikeda, T.; Terakura, K.; Ozaki, J. I.; Miyata, S. *J. Power Sources* **2009**, *187*, 93.
(102) Okamoto, Y. *Appl. Surf. Sci.* **2009**, *256*, 335.
(103) Tsai, C. W.; Tu, M. H.; Chen, C.-J.; Hung, T. F.; Liu, R. S.; Liu, W. R.; Lo, M. Y.; Peng, Y. M.; Zhang, L.; Zhang, J.; Shy, D. S.; Xing, X. K. *RSC Adv.* **2011**, *1*, 1349.
(104) Liang, Y.; Li, Y.; Wang, H.; Zhou, J.; Wang, J.; Regier, T.; Dai, H. *Nat. Mater.* **2011**, *10*, 780.
(105) Avouris, P.; Chen, Z.; Perebeinos, V. *Nat. Nanotechnol.* **2007**, *2*, 605.
(106) Schwierz, F. *Nat. Nanotechnol.* **2010**, *5*, 487.
(107) Wei, X. L.; Fang, H.; Wang, R. Z.; Chen, Y. P.; Zhong, J. X. *Appl. Phys. Lett.* **2011**, *99*, 012107.
(108) Son, Y. W.; Cohen, M. L.; Louie, S. G. *Phys. Rev. Lett.* **2006**, *97*, 216803.
(109) Yu, S. S.; Zheng, W. T.; Wen, Q. B.; Jiang, Q. *Carbon* **2008**, *46*, 537.
(110) Li, Y.; Zhou, Z.; Shen, P.; Chen, Z. *ACS Nano* **2009**, *3*, 1952.
(111) Biel, B.; Blase, X.; Triozon, F.; Roche, S. *Phys. Rev. Lett.* **2009**, *102*, 096803.
(112) Perebeinos, V.; Tersoff, J.; Avouris, P. *Phys. Rev. Lett.* **2005**, *94*, 027402.
(113) Zhou, X.; Park, J. Y.; Huang, S.; Liu, J.; McEuen, P. L. *Phys. Rev. Lett.* **2005**, *95*, 146805.
(114) Pan, D.; Wang, S.; Zhao, B.; Wu, M.; Zhang, H.; Wang, Y.; Jiao, Z. *Chem. Mater.* **2009**, *21*, 3136.
(115) Wu, Z. S.; Ren, W.; Xu, L.; Li, F.; Cheng, H. M. *ACS Nano* **2011**, *5*, 5463.
(116) Wang, H.; Zhang, C.; Liu, Z.; Wang, L.; Han, P.; Xu, H.; Zhang, K.; Dong, S.; Yao, J.; Cui, G. *J. Mater. Chem.* **2011**, *21*, 5430.
(117) Cho, Y. J.; Kim, H. S.; Im, H.; Myung, Y.; Jung, G. B.; Lee, C. W.; Park, J.; Park, M. H.; Cho, J.; Kang, H. S. *J. Phys. Chem. C* **2011**, *115*, 9451.
(118) Jia, L.; Wang, D. H.; Huang, Y. X.; Xu, A. W.; Yu, H. Q. *J. Phys. Chem. C* **2011**, *115*, 11466.